PAPER

Check for updates

Roll-to-roll sputtered and patterned Cu$_{2-x}$O/Cu/Cu$_{2-x}$O multilayer grid electrode for flexible smart windows†

Hyeong-Jin Seo,[a] Yoon-Chae Nah[b] and Han-Ki Kim [ID] *[a]

We fabricated cost-effective Cu$_{2-x}$O/Cu/Cu$_{2-x}$O multilayer grid electrodes using roll-to-roll (RTR) sputtering and patterning processes for use as transparent and flexible electrodes in flexible smart windows. To optimize the patterned Cu$_{2-x}$O/Cu/Cu$_{2-x}$O multilayer grid, the electrical and optical properties of the Cu$_{2-x}$O/Cu/Cu$_{2-x}$O multilayer grid electrodes were investigated as a function of grid width and pitch, which directly influence the filling factor of the grid. At the optimized grid width of 16 and pitch of 600 μm, the Cu$_{2-x}$O/Cu/Cu$_{2-x}$O multilayer grid had a sheet resistance of 7.17 Ohm per square and an optical transmittance of 87.6%. In addition, the mechanical properties of the optimized Cu$_{2-x}$O/Cu/Cu$_{2-x}$O multilayer grid electrode was compared to those of brittle ITO electrodes to demonstrate its outstanding flexibility. To show the potential of the Cu$_{2-x}$O/Cu/Cu$_{2-x}$O multilayer grid for smart windows, we fabricated a flexible and transparent thin film heater (TFH) and a flexible electrochromic (EC) device, which are key components of smart windows. The low saturation voltage of the Cu$_{2-x}$O/Cu/Cu$_{2-x}$O grid-based TFH and the fast on−off performance of the Cu$_{2-x}$O/Cu/Cu$_{2-x}$O grid-based EC device indicates that the RTR-processed Cu$_{2-x}$O/Cu/Cu$_{2-x}$O multilayer grid is promising as a low-cost and large-area flexible transparent electrode for high-performance smart windows.

1. Introduction

Multi-functional smart windows equipped with transparent displays, transparent heaters, electrochromic devices, and energy-harvesting devices have attracted significant attention as next-generation exterior materials for buildings and automobiles.[1–5] Unlike conventional windows, which simply pass visible light into the building or automobile, smart windows provide several convenient and smart functions, such as information displays, energy harvesting, self-heating and cleaning, transmittance control, and indoor temperature and light control. In several components of smart windows, flexible and transparent thin film heaters (TFHs) can remove frost or ice by heating the window and flexible electrochromic (EC) devices, which can adjust the indoor brightness by controlling the transmittance of the window.[5–7] The performance, stability, and fabrication cost of TFHs and EC devices are critically dependent on the electrical, optical, and mechanical properties of transparent and flexible electrodes (TFEs). In addition, the

fabrication cost of TFHs and EC devices for low-cost and large-area smart windows is closely related to the cost of the TFE materials and coating processes. Therefore, the development of highly transparent, conductive, flexible, and cost-effective TFE materials and processing methods is imperative for mass-producing TFHs and EC devices. A common transparent conducting electrode (TCE) material, Sn-doped In$_2$O$_3$ (ITO) films coated on polyethylene terephthalate (PET) substrates are typically employed as TFEs due to their low sheet resistance, high optical transmittance, well-known processing technology, and ease of use for large-area coatings.[8–12] However, sputtered ITO films are critically limited as high-quality and cost-effective TFEs due to the relatively high sheet resistance and poor mechanical properties of ITO/PET films as well as the high cost of indium.[13] Several TCE materials fabricated by vacuum-based or solution-based coating processes have been extensively reported as replacements for high-cost ITO films.[14–19] Among these, sputtered oxide–metal–oxide (OMO) multilayer films and printed metal (Ag, Cu) grid electrodes are considered to be promising replacements. However, sputtered OMO electrodes are still composed of high-cost indium-based oxide and Ag interlayers. In the case of the printed metal grid electrodes, the patterned grid is shiny due to the high reflection on the surface. To solve both of these problems, it is necessary to develop a cost-effective OMO-based multilayer grid electrode that combines the merits of the OMO and the metal grid.

[a]School of Advanced Materials Science & Engineering, Sungkyunkwan University, 2066 Seobu-ro, Jangan-gu, Suwon, Gyeonggi-do, 440-746, Republic of Korea. E-mail: hankikim@skku.edu; Fax: +82-31-290-7410; Tel: +82-31-290-7390

[b]IPCE, Dept. of Energy, Materials, and Chemical Engineering, Korea University of Technology and Education, Cheonan 31253, Republic of Korea

† Electronic supplementary information (ESI) available. See DOI: 10.1039/c8ra03252a

In this work, we developed a grid-patterned OMO multilayer electrode with a $Cu_{2-x}O/Cu/Cu_{2-x}O$ structure using a lab-scale roll-to-roll (RTR) sputtering system to replace high-cost ITO electrodes. To optimize the grid width and pitch of the $Cu_{2-x}O/Cu/Cu_{2-x}O$ multilayer grid, we investigated the electrical and optical properties of the $Cu_{2-x}O/Cu/Cu_{2-x}O$ multilayer grid as a function of grid width and pitch. In addition, the mechanical properties of the $Cu_{2-x}O/Cu/Cu_{2-x}O$ multilayer as a substitute for a typical sputtered ITO electrode were comprehensively investigated using lab-designed outer and inner bending tests. Furthermore, we used our patterned OMO multilayer grid electrode to fabricate flexible TFHs and EC devices to demonstrate their feasibility for application in next-generation flexible smart windows.

2. Experimental

2.1 Continuous roll-to-roll sputtering and patterning of $Cu_{2-x}O/Cu/Cu_{2-x}O$ multilayer grid on a PET substrate

A $Cu_{2-x}O/Cu/Cu_{2-x}O$ multilayer was deposited on a 125 μm-thick PET substrate (Kimoto Ltd., Japan) using a lab-scale RTR sputtering system with a linear ion gun and linear cathodes. Using a Cu rectangular target with a size of 460 mm × 130 mm, the Cu-deficient $Cu_{2-x}O$ layer was deposited by reactive sputtering in an Ar/O_2 ambient atmosphere and the Cu layer was deposited by DC sputtering in a pure Ar ambient atmosphere in the same RTR chamber. In detail, a 150 nm-thick bottom $Cu_{2-x}O$ layer was directly sputtered on the PET substrate after treating it with an Ar beam. The Cu layer was reactively sputtered on the PET substrate at a constant rolling speed of 0.4 m min^{-1} by applying a DC power of 2.2 kW to a Cu target under Ar/O_2 gas with a flow rate of 400/120 sccm. A 150 nm-thick Cu interlayer was then sputtered on the bottom $Cu_{2-x}O$ layer at a DC power of 2.2 kW under a pure Ar gas flow of 450 sccm. Finally, the top $Cu_{2-x}O$ layer was reactively sputtered on the Cu metal interlayer under the same sputtering conditions as the bottom $Cu_{2-x}O$ layer. Fig. 1(a) shows a schematic of the RTR sputtering process for the $Cu_{2-x}O/Cu/Cu_{2-x}O$ multilayer. Due to the semi-transparency of the $Cu_{2-x}O$ layer and the opacity of the Cu layer, the as-deposited $Cu_{2-x}O/Cu/Cu_{2-x}O$ multilayer had a dark brown color with an optical transmittance of 0% (ESI Fig. S1†). To pattern the opaque $Cu_{2-x}O/Cu/Cu_{2-x}O$ multilayer, a liquid photoresist (LPR) layer was coated on the sputtered $Cu_{2-x}O/Cu/Cu_{2-x}O$ multilayer using a commercial slot die coating system. The LPR-coated $Cu_{2-x}O/Cu/Cu_{2-x}O$ multilayer was passed to a heating chamber by means of an unwinding and rewinding roller. The $Cu_{2-x}O/Cu/Cu_{2-x}O$ multilayer was exposed to ultraviolet (UV) light using a positive grid mask with varying grid width and pitch. After UV irradiation, the $Cu_{2-x}O/Cu/Cu_{2-x}O$ multilayer was patterned using a developing solution (DN-DT238E). Then, the photolithographed $Cu_{2-x}O/Cu/Cu_{2-x}O$ multilayer was wet-etched using an etching solution (0.5% $FeCl_3$ in deionized water) to form the grid structure. The wet-etched $Cu_{2-x}O/Cu/Cu_{2-x}O$ multilayer was then stripped using a stripping solution. The stripped $Cu_{2-x}O/Cu/Cu_{2-x}O$ multilayer grid was rinsed with deionized water. Fig. 1(b) shows the roll-to-roll patterning process for the
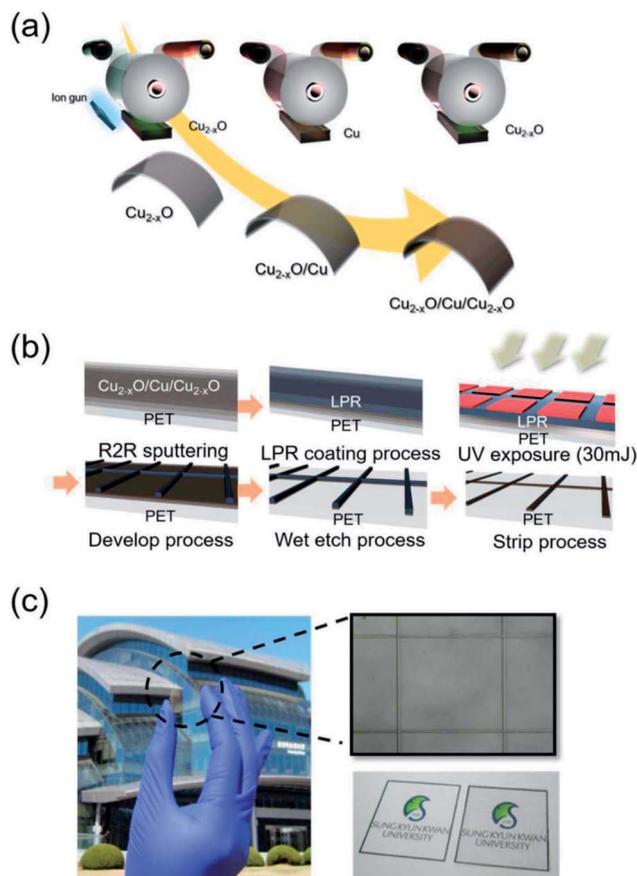

Fig. 1 (a) Schematics of roll-to-roll sputtering and (b) roll-to-roll patterning of the $Cu_{2-x}O/Cu/Cu_{2-x}O$ multilayer grid prepared on a PET substrate. (c) Picture of the grid-patterned $Cu_{2-x}O/Cu/Cu_{2-x}O$ multilayer and optical microscope image of the patterned grid electrode.

$Cu_{2-x}O/Cu/Cu_{2-x}O$ multilayer grid. The patterned $Cu_{2-x}O/Cu/Cu_{2-x}O$ grid had high optical transmittance due to the narrow grid width and wide pitch, as shown in Fig. 1(c), unlike the as-deposited $Cu_{2-x}O/Cu/Cu_{2-x}O$ films with dark brown color. The electrical and optical properties of the $Cu_{2-x}O/Cu/Cu_{2-x}O$ multilayer grid electrode were investigated as a function of grid width and pitch using Hall measurements (HL5500PC, Accent Optical Technology) and a UV/visible spectrometer (UV 540, Unicam). In addition, the composition and binding energy of the reactive sputtered $Cu_{2-x}O$ film in the multilayer grid electrode were analyzed by using X-ray photoelectron spectroscopy (XPS: ESCALAB250). The mechanical properties of the grid-patterned $Cu_{2-x}O/Cu/Cu_{2-x}O$ multilayer were evaluated using a specially designed inner and outer bending system. In addition, a dynamic fatigue bending test was performed using a lab-designed cyclic bending system operating at 0.5 Hz for 10 000 cycles.

2.2 Fabrication and evaluation of thin film heaters and electrochromic devices

To demonstrate the potential of the grid-patterned $Cu_{2-x}O/Cu/Cu_{2-x}O$ multilayer, we fabricated flexible TFHs and EC

devices on an optimized $Cu_{2-x}O/Cu/Cu_{2-x}O$ multilayer grid electrode. Flexible TFHs with size of 25×25 mm^2 with two-terminal side contacts was fabricated on the $Cu_{2-x}O/Cu/Cu_{2-x}O$ multilayer grid (Fig. S2†). A 200 nm-thick Ag side contact electrode was sputtered onto the edge of the grid, and a DC voltage was supplied by a power supply (OPS 3010, ODA Technologies) to the grid-based TFHs through the Ag contact electrode at the film edge. The temperature of the TFHs was measured using a thermocouple mounted on their surface and an infrared (IR) thermal imager (A35sc, FLIR). Fig. S3† shows a picture of the temperature measurement system, including the thermocouple and IR thermal imager. A commercial ITO electrode with sheet resistance of 38.27 Ohm per square and optical transmittance of 87.52% was used as a reference. We also fabricated flexible electrochromic devices on the optimized $Cu_{2-x}O/Cu/Cu_{2-x}O$ multilayer grid electrode. Prior to the deposition of poly(3-hexylthiophene) (P3HT), a poly(3,4-ethylenedioxythiophene):polystyrene sulfonate (PEDOT:PSS) film (NanoWearable Co.) was spin-coated at 1500 rpm for 30 s and cured at 120 °C for 5 min. A 2.2 wt% solution of P3HT (Aldrich) in chlorobenzene (Aldrich) was spin-coated on the PEDOT:PSS/grid substrates at 1500 rpm for 20 s and then dried on a hot plate at 60 °C for 10 min. The thickness of the P3HT films was around 60 nm, as measured using a fused ion beam-scanning electron microscope (FIB-SEM) (Helios NanoLab 600i). Electrochromic tests were performed in a three-electrode system with a propylene carbonate solution containing 0.5 M LiClO$_4$. The working electrode was the P3HT film on a grid electrode. Pt wire and Ag/Ag$^+$ wire were used as the counter and reference electrodes, respectively. The potential of the samples was controlled using a potentiostat/galvanostat (PGSTAT 302N, Autolab) and the optical properties of P3HT were measured using a UV/vis spectrometer (Cary 100, Agilent Technologies). The pulse potential tests were carried out by applying -0.2 V for coloring and 0.8 V for bleaching. Each coloring and bleaching time was set to 60 s.

3. Results and discussion

To investigate the stoichiometry and phase of the copper oxide fabricated by RTR sputtering, we carried out XPS analysis for the top Cu$_2$O layer in the $Cu_{2-x}O/Cu/Cu_{2-x}O$ multilayer grid. Fig. 2

shows the XPS core level spectra of the Cu 2p peaks and the O 1s peaks obtained from $Cu_{2-x}O/Cu/Cu_{2-x}O$ grid multilayer film. In general, reactive sputtered Cu could form two different oxides, such as cuprous oxide (Cu$_2$O) and cupric oxide (CuO), depending on the oxygen flow ratio.[20,21] The binding energies of the Cu 2p$_{1/2}$ (951.43 eV) and 2p$_{3/2}$ (931.38 eV) were matched with general cuprous Cu$_2$O phase.[22,23] The O 1s peak at 530.38 eV was also matched with cuprous Cu$_2$O phase.[24] In addition, XPS analysis showed that the RTR sputtered Cu$_2$O phase had a Cu-deficiency (Cu/O ratio: 1.88–1.92). Therefore, we concluded that the multilayer grid was consisted of top and bottom $Cu_{2-x}O$ phase. In our previous work, we also confirmed the cuprous Cu$_2$O phase of the reactive RTR sputtered copper oxide films using XRD and TEM examinations.[23]

Thickness of each layer in the $Cu_{2-x}O/Cu/Cu_{2-x}O$ multilayer grid electrodes was determined by consideration of optical transmittance, conductivity and adhesion of the multilayer grid. Generally, the high reflection from Cu metal interlayer resulted in glittering of the Cu grid, which prevent the use of Cu grid electrode for large area smart window. However, covering of 150 nm thick black $Cu_{2-x}O$ layer on the Cu interlayer could effectively reduce the reflection from Cu layer. Due to existence of the thick $Cu_{2-x}O$ layer led to no glittering from the $Cu_{2-x}O/Cu/Cu_{2-x}O$ multilayer grids. In case of 150 nm thick bottom $Cu_{2-x}O$ layer, it improved adhesion of the $Cu_{2-x}O/Cu/Cu_{2-x}O$ multilayer grid with PET substrate. Because reactive sputtered $Cu_{2-x}O$ layer sandwiched the Cu metal interlayer has a semi-conducting property, the thick Cu metallic layer is necessary in the multilayer grid electrode for obtaining a low sheet resistance comparable to typical metal grid electrodes.

Fig. 3 shows the sheet resistance and resistivity of the patterned $Cu_{2-x}O/Cu/Cu_{2-x}O$ multilayer grid electrodes as a function of grid line width and pitch. In general, the electrical and optical properties of metal grid electrodes are critically dependent on the geometry of the grid, such as the grid width, grid height, and pitch.[25–27] Therefore, it is very important to optimize the grid width and pitch to obtain low sheet resistance and high transmittance. Fig. 3(a)–(d) show the sheet resistance and resistivity of the $Cu_{2-x}O/Cu/Cu_{2-x}O$ multilayer grid electrodes at a specific grid width (10, 12, 14, and 16 μm) with increasing pitch length. Each inset shows the geometry of the constant grid width. It is clear that the sheet resistance and
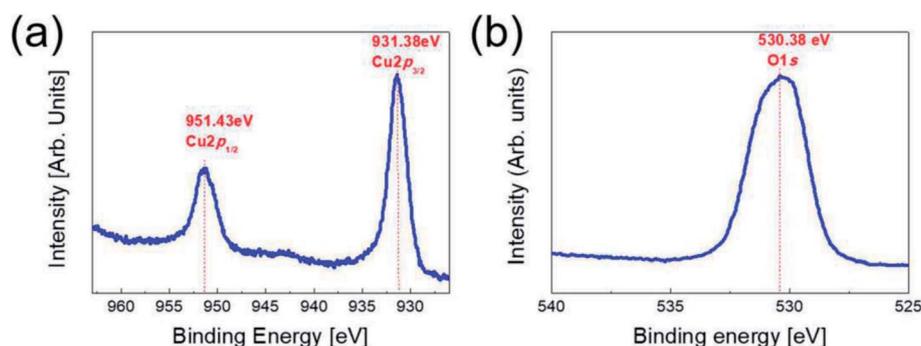

Fig. 2 Core level spectra of (a) the Cu 2p peaks (b) the O 1s peak obtained from top $Cu_{2-x}O$ layer in the $Cu_{2-x}O/Cu/Cu_{2-x}O$ multilayer grid.
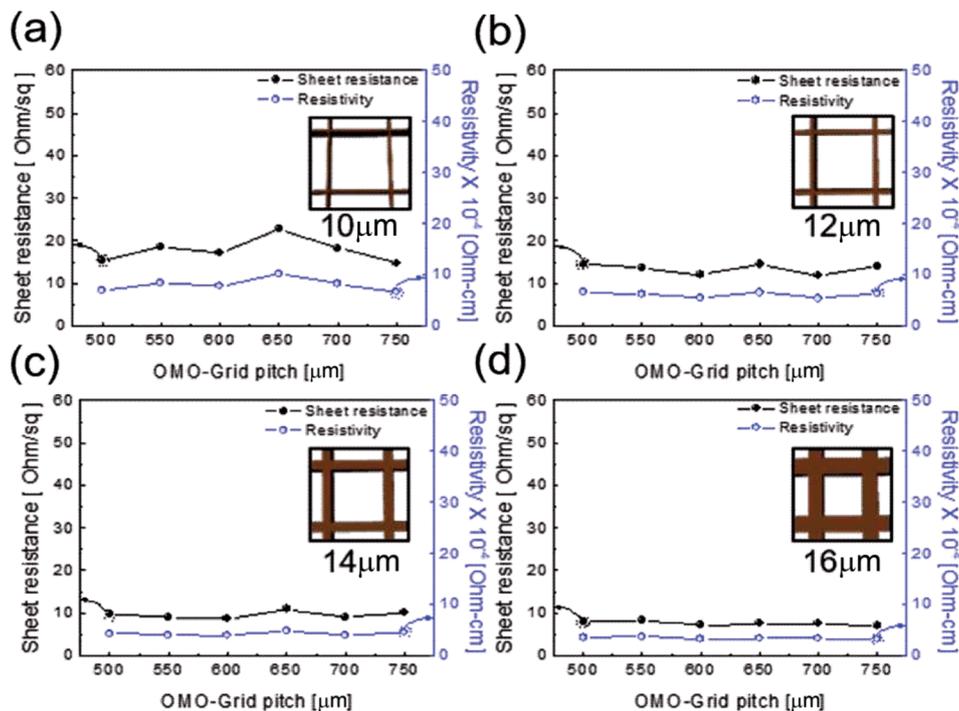
Fig. 3 Sheet resistance and resistivity of the $Cu_{2-x}O/Cu/Cu_{2-x}O$ multilayer grid electrode as a function of pitch length at a constant grid width of (a) 10, (b) 12, (c) 14, and (d) 16 μm. The inset shows the constant grid width.

resistivity of the $Cu_{2-x}O/Cu/Cu_{2-x}O$ multilayer grid electrode decreased with increasing grid width from 10 to 16 μm. However, the grid pitch did not affect the sheet resistance or resistivity; with increasing grid pitch length from 500 to 750 μm, the grid electrode showed similar sheet resistance and resistivity because the changes in grid pitch were small. At a grid width of 16 μm, the $Cu_{2-x}O/Cu/Cu_{2-x}O$ multilayer grid showed the lowest sheet resistance of 7.69 ± 0.59 Ohm per square and resistivity of $3.46 \pm 0.2 \times 10^{-4}$ Ohm cm^{-1}. Due to the existence of the conductive Cu interlayer, the $Cu_{2-x}O/Cu/Cu_{2-x}O$ multilayer grid exhibited better metallic conductivity than a typical ITO electrode. The calculated resistivity of the Cu interlayer was found to be 3.0×10^{-6} Ohm cm^{-1}, which is similar to that of bulk Cu (1.7×10^{-6} Ohm cm^{-1}).[23] Therefore, the grid width of the Cu interlayer affected the electrical properties of the $Cu_{2-x}O/Cu/Cu_{2-x}O$ multilayer grid because it provides the main current path.

Fig. 4 shows the optical transmittance of the $Cu_{2-x}O/Cu/Cu_{2-x}O$ multilayer grid electrode as a function of grid width and pitch length. With increasing grid width and decreasing pitch length, the optical transmittance decreased, as shown in Fig. 4(a)–(d). At grid widths of 10 and 12 μm, the optical transmittance of the $Cu_{2-x}O/Cu/Cu_{2-x}O$ multilayer grid electrode was almost constant regardless of grid pitch between 500 and 750 μm, as shown in Fig. 4(a) and (b). However, at grid widths of 14 and 16 μm, the optical transmittance of the multilayer grid was affected by pitch length. The optical transmittance of the electrode began to decrease at a grid pitch of 550 μm. Therefore, to obtain a high-performance multilayer grid electrode, the grid pitch should be larger than 550 μm. In the

$Cu_{2-x}O/Cu/Cu_{2-x}O$ multilayer grid electrodes, a high conductivity was determined by width of the metallic Cu layer because top and bottom $Cu_{2-x}O$ layers had semiconducting properties unlike typical OMO electrodes where the oxide layer is highly conductive oxide layer. In addition, the optical transmittance of the $Cu_{2-x}O/Cu/Cu_{2-x}O$ grid electrode was dependent on the uncovered space in the grid structure because the $Cu_{2-x}O/Cu/Cu_{2-x}O$ multilayer had an optical transmittance of 0% (Fig. S1†). Therefore, appropriate design of grid structure and geometry is very important to obtain high-quality multilayer grid electrodes.

To determine the optimum grid width and pitch length of the $Cu_{2-x}O/Cu/Cu_{2-x}O$ multilayer grid electrodes for flexible smart windows, the figure of merit (FOM; T^{10}/R_{sh}), as defined by Haacke,[28] was evaluated from the measured sheet resistance (R_{sh}) and optical transmittance (T) at a wavelength of 550 nm. As shown in Fig. 5(a) and (b), for very thin grid widths below 12 μm, the $Cu_{2-x}O/Cu/Cu_{2-x}O$ multilayer grid electrode had a similar FOM value regardless of grid pitch length. The 12 μm grid showed slightly increased FOM values compared to the 10 μm grid due to the slightly decreased sheet resistance. However, at grid pitches of 14 and 16 μm, the FOM of the $Cu_{2-x}O/Cu/Cu_{2-x}O$ multilayer grid was affected by grid pitch, as shown in Fig. 5(c) and (d). Due to the low optical transmittance, the grid had a low FOM at grid pitch lengths of 500 and 550 μm. The $Cu_{2-x}O/Cu/Cu_{2-x}O$ multilayer with a grid width of 16 μm had the highest FOM (37.34×10^{-3} Ohm^{-1}) at a grid pitch length of 600 μm. The grid width and pitch length dependence can be explained by the filling factor (f_F) of the $Cu_{2-x}O/Cu/Cu_{2-x}O$ multilayer grid. We calculated f_F as follows. Ghosh *et al.*

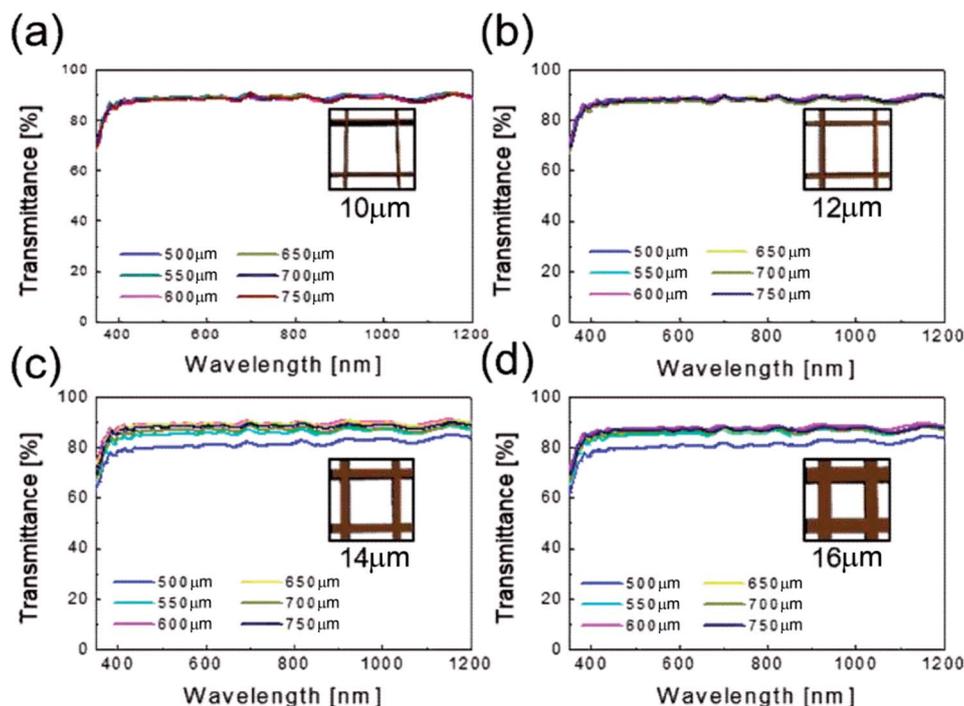**Fig. 4** Optical transmittance of the $Cu_{2-x}O/Cu/Cu_{2-x}O$ multilayer grid electrodes as a function of pitch length at a constant grid width of (a) 10, (b) 12, (c) 14, and (d) 16 μm.

reported that a Ni grid electrode has low sheet resistance and high optical transmittance at a fill factor of 0.025.[27]

$$f_F = \frac{W}{(G + W)} = 0.025$$

here, W and G are the widths and grid pitch of the $Cu_{2-x}O/Cu/Cu_{2-x}O$ multilayer grid electrode. Given that the grid width was 16 μm, the highest FOM for the $Cu_{2-x}O/Cu/Cu_{2-x}O$ multilayer grid is obtained at $G = 600$ μm, with an f_F value of 0.0259. This calculated value matched the measured value, as shown in
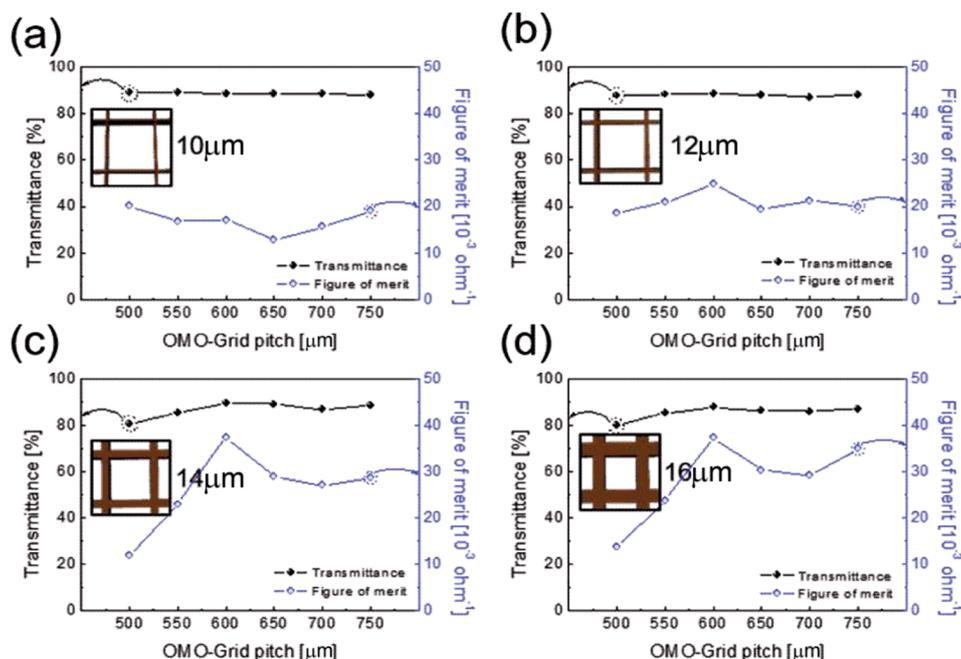
Fig. 5 Figure of merit of the $Cu_{2-x}O/Cu/Cu_{2-x}O$ multilayer grid electrode, calculated from the sheet resistance and optical transmittance at a 550 nm wavelength. The figure of merit is given as a function of pitch length at constant grid widths of (a) 10, (b) 12, (c) 14, and (d) 16 μm.

Fig. 9   (a) Schematics of the $Cu_{2-x}O/Cu/Cu_{2-x}O$ multilayer grid-based TFHs, mounted in a special jig before and after heating by applied DC power. Temperature plot of flexible TFH fabricated on (b) the $Cu_{2-x}O/Cu/Cu_{2-x}O$ multilayer grid electrode as a function of applied voltage. The inset is an IR image of the flexible thin film heater at an applied voltage of 5.5 V. (c) Temperature plot of the ITO-based flexible thin film heater, reaching 100 °C at an applied voltage of 10.5 V.

in Fig. 9(a). The flexible TFHs were fabricated with a size of 25 × 25 mm^2 using a two-terminal Ag contact configuration (Fig. S2†). A DC voltage was applied to the TFHs through the sputtered Ag metal contact electrodes at the film edge, and the temperature profiles were measured using a thermocouple placed on the surface and an IR thermometer (Fig. S3†). A flexible TFH was mounted on a specially designed sample jig to supply power and measure the temperature. Fig. 9(b) shows the temperature profiles of the TFHs with $Cu_{2-x}O/Cu/Cu_{2-x}O$ multilayer grid electrodes, plotted with respect to input voltage from 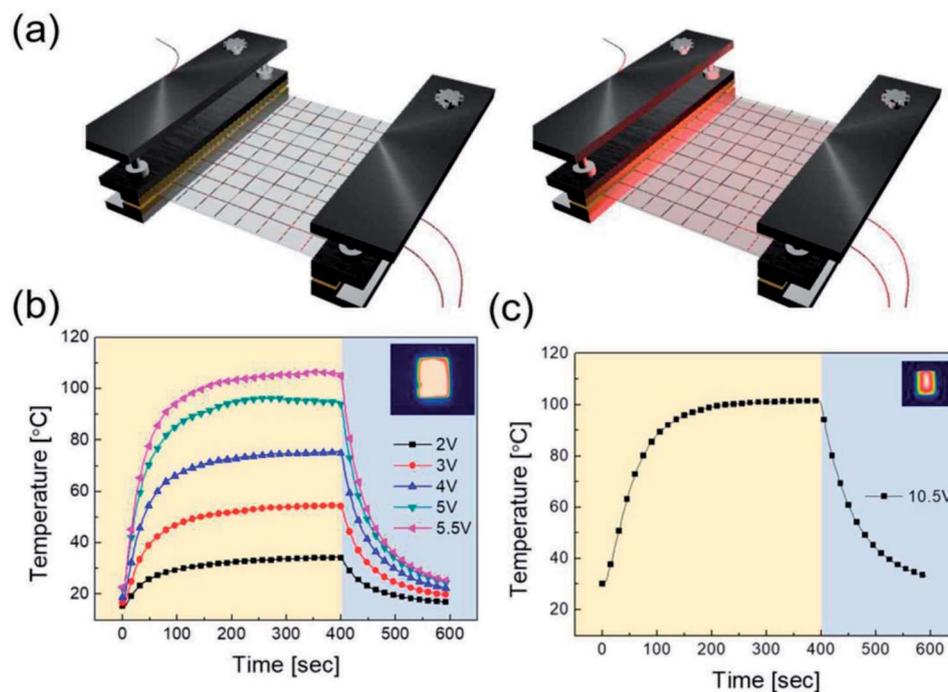2 to 5.5 V. Generally, as the input voltage increased, the saturation temperature of the TFHs increased. Due to the low sheet resistance (7.18 Ohm per square) of the $Cu_{2-x}O/Cu/Cu_{2-x}O$ multilayer grid electrode, the flexible TFHs on the electrode with a width of 16 μm and pitch length of 600 μm reached a saturation temperature of 100 °C when a low DC input voltage of 5.5 V was applied. The higher saturation temperature of the flexible TFHs with $Cu_{2-x}O/Cu/Cu_{2-x}O$ multilayer grid electrodes at low input voltage implies that efficient transduction of electric energy through Joule heating occurred. Based on Joule's law, the saturation temperature of the flexible TFHs can be expressed as follows.

$$T_s = \frac{V^2 \Delta t}{R h_{conv} A_{conv}} + T_i$$

The power (P) applied to the flexible TFHs over a heating time (Δt) generates heat in the TFH, as illustrated in Fig. 9(a). In the above equation, V is the applied voltage, R is the device

resistance, h_{conv} is the heat transfer coefficient, A_{conv} is the surface area, and T_s and T_i are the saturation and initial temperatures. Therefore, it is apparent that the saturation temperature of flexible TFHs increases with increasing input voltage (V) and with decreasing resistance (R). Therefore, the low sheet resistance of the $Cu_{2-x}O/Cu/Cu_{2-x}O$ multilayer grid electrode mainly results in the rapid attainment of a saturation temperature of 100 °C even at low voltage, which is appropriate for removing frost or deicing a smart window. On the other hand, the flexible TFH fabricated on an ITO electrode reached the saturation temperature of 100 °C at a higher input voltage of 10.5 V due to the higher sheet resistance (38.27 Ohm per square) of the sputtered ITO film. Although the ITO-based TFH did reach a temperature of 100 °C, it cannot be applied to flexed or specially shaped surfaces due to the brittleness of the sputtered ITO films. This indicates that the roll-to-roll sputtered and patterned $Cu_{2-x}O/Cu/Cu_{2-x}O$ multilayer grid electrode is a promising flexible TCE for an effective transparent defroster in smart windows. It could be employed as a defogging/deicing window in automobiles, helmets, and smart windows due to its flexibility and transparency. To investigate the durability of $Cu_{2-x}O/Cu/Cu_{2-x}O$ multilayer grid in the flexible TFHs, we performed repeated heating–cooling tests for 10 cycles. Fig. 10(a) shows the temperature profiles of the $Cu_{2-x}O/Cu/Cu_{2-x}O$ multilayer grid-based TFHs for 10 repeated cycles. The $Cu_{2-x}O/Cu/Cu_{2-x}O$ multilayer grid-based TFHs showed identical temperature profiles, rapidly reaching a saturation temperature of 100 °C when a DC voltage of 5.2 V was applied. Fig. 10(b) and (c) compared the sheet resistance and optical
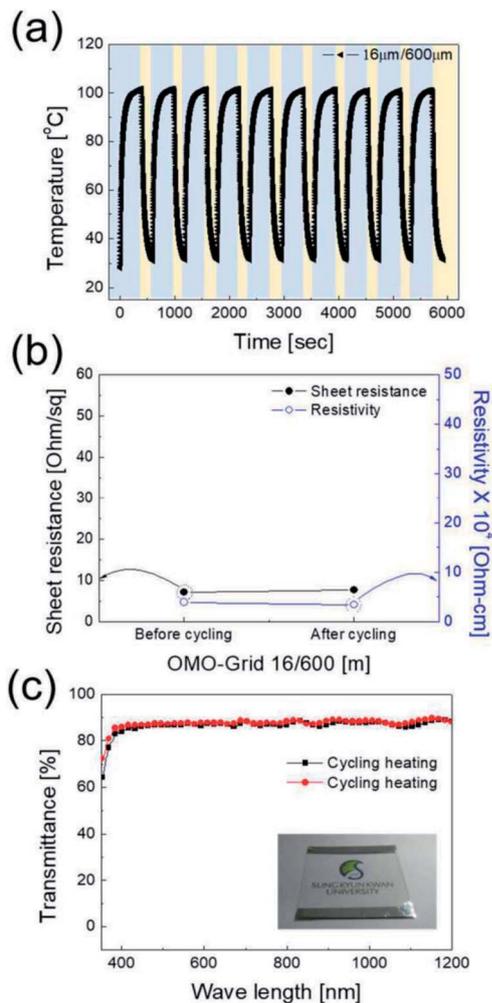
Fig. 10 (a) Repeated heating and cooling cycles of the optimized $Cu_{2-x}O/Cu/Cu_{2-x}O$ multilayer grid (600 μm grid pitch/16 μm grid width)-based thin film heater to show the stability of the $Cu_{2-x}O/Cu/Cu_{2-x}O$ grid electrode. (b) Sheet resistance, resistivity, and (c) optical transmittance of $Cu_{2-x}O/Cu/Cu_{2-x}O$ multilayer grid electrode on the TFHs before and after repeated 10 times heating–cooling cycles.

Fig. 11 (a) Absorbance spectra for the P3HT/PEDOT:PSS film on the $Cu_{2-x}O/Cu/Cu_{2-x}O$ multilayer grid electrode. The inset shows the colored and bleached states of the sample. (b) *In situ* transmittance spectra for P3HT/PEDOT:PSS film measured at 520 nm and 720 nm when a voltage pulse was applied with an interval of 60 s. (c) Change in transmittance (ΔT) as a function of oxidation potential.

transmittance change before and after heating and cooling cycling test. Similar sheet resistance and optical transmittance of the $Cu_{2-x}O/Cu/Cu_{2-x}O$ multilayer grid electrode indicates stability of the RTR sputtered $Cu_{2-x}O/Cu/Cu_{2-x}O$ multilayer grid electrodes. Inset picture in Fig. 10(c) showed the identical transmittance of the TFH with $Cu_{2-x}O/Cu/Cu_{2-x}O$ multilayer grid electrode after 10 times heating and cooling cycling.

The electrochromic absorption of the flexible P3HT/PEDOT:PSS film was monitored by UV-vis spectroscopy at different applied voltages. A series of spectroelectrochemical spectra for the sample are shown in Fig. 11(a). When a potential of from −0.2 V to 0.8 V was applied (oxidation reaction), the absorption peak at around 520 nm decreased and a new band formed around 700 nm. During this reaction, the color of the film became lighter, changing from its original red color and eventually becoming transparent blue with the formation of bipolaronic P3HT (see inset of Fig. 11(a)).[30,31] During the reverse scan from 0.8 V to −0.2 V, the reduction reaction occurred and
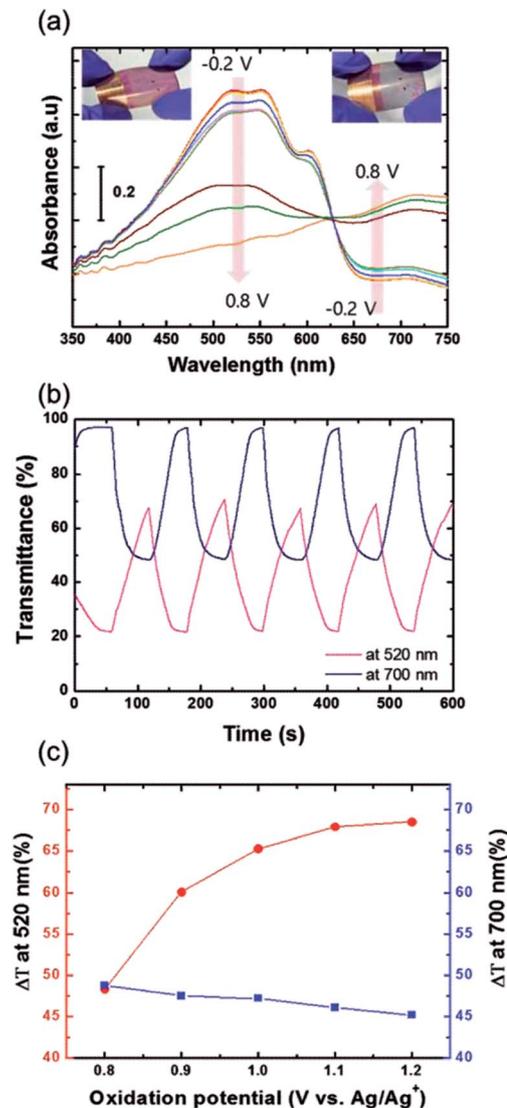
the P3HT films recovered their original red color. In the initial stages of the electrochemical reaction in this voltage range, the electrochromic coloration was stable without any degradation of the polymer films. However, the P3HT film coated directly on a grid substrate did not show any color change during the electrochemical reactions when a potential from −0.2 V to 0.7 V was applied, as shown in Fig. S4(a).† The abrupt decay in the absorption spectra at 0.8 V might be attributed to partial dissolution of the P3HT film due to a high electric field locally concentrated on the grid. These findings indicate that coating the $Cu_{2-x}O/Cu/Cu_{2-x}O$ multilayer grid electrode with a conductive PEDOT:PSS layer homogenized the electric field in the film, and that the P3HT film was found to enable electrochemically stable optical modulation at the given potential.[32] Although PEDOT is well known to be a cathodically coloring

material with strong blue absorption,[33] the PEDOT:PSS layer was optically inactive during electrochemical reactions between −0.2 and 0.8 V (Fig. S4(b)†), which implies that the electrochromic absorption of the P3HT/PEDOT:PSS film entirely originated from the P3HT layer. Fig. 11(b) presents the transmittance data for a P3HT film during cyclic potential switching between −0.2 V and 0.8 V. The differences in transmittance (ΔT) were 48.3% and 48.8% measured at 520 nm and 700 nm, respectively. When the oxidation potential was extended to 1.2 V (as shown in Fig. 11(c)), ΔT at 520 nm gradually increased to 68.5%, while ΔT at 700 nm was almost the same or slightly decreased. This means that the main absorption peak of the P3HT film located at 520 nm could be modulated by extending the oxidation potential. In particular, the bleached P3HT film under 1.2 V of oxidation potential was highly transparent, with 91.4% of transmittance (Fig. S5†). The response times during the bleaching (τ_b) and coloring (τ_c) processes were estimated as the time to reach 90% of the total transmittance difference. The τ_b and τ_c measured at 520 nm were 49.5 s and 30.4 s, respectively. Compared to EC devices with silver grid substrates,[34] these values are quite reasonable with a high ΔT, but could be improved by further optimization of grid geometry or of the conductive PEDOT:PSS layer.

4. Conclusions

In summary, we developed a $Cu_{2-x}O/Cu/Cu_{2-x}O$ multilayer grid electrode for TFHs and electrochromic devices using roll-to-roll sputtering and patterning processes at room temperature. The optimized $Cu_{2-x}O/Cu/Cu_{2-x}O$ multilayer grid electrodes exhibited a low sheet resistance of 7.17 Ohm per square and high optical transmittance of 87.6%. In addition, we found that the $Cu_{2-x}O/Cu/Cu_{2-x}O$ multilayer grid had outstanding flexibility due to the high flexibility of the Cu interlayer. The mechanical stability of the $Cu_{2-x}O/Cu/Cu_{2-x}O$ multilayer grid was compared with that of a commercial ITO electrode using inner/outer bending and fatigue tests. Due to the lower sheet resistance of the electrode, the flexible TFH with the transparent $Cu_{2-x}O/Cu/Cu_{2-x}O$ multilayer grid required a lower input voltage (5.5 V) to reach a saturation temperature of 100 °C than the ITO-based TFHs. Furthermore, a P3HT film coated on a $Cu_{2-x}O/Cu/Cu_{2-x}O$ substrate exhibited efficient coloring/bleaching performance. The temperature profiles and EC properties indicate that the $Cu_{2-x}O/Cu/Cu_{2-x}O$ multilayer grid electrode is a promising TCE for flexible smart windows.

Conflicts of interest

The authors declare no competing financial interests.

Acknowledgements

References

1 B. Clemens, F. Suzanne, Z. Arie, S. Julian and G. A. Brian, *Nature*, 1996, **383**, 608–610.

2 W. Kai, W. Haiping, M. Yuena, Z. Yajie and W. Zhixiang, *Energy Environ. Sci.*, 2012, **5**, 8384–8389.

3 X. Zhong, J. Xiujuan, C. Gui, X. Jing, C. Di and S. Guozhen, *Chem. Commun.*, 2014, **50**, 608–610.

4 C. Guofa, D. Peter, C. Xing and L. Pooi See, *Adv. Energy Mater.*, 2017, **7**, 1602598.

5 L. Sen, B. Xiaopeng, W. Haiyang, W. Haolun, S. Jianan, H. Kai, W. Chang, W. Ning, L. Bo, L. Ming and W. Hui, *Adv. Mater.*, 2017, **29**, 1703238.

6 T. Naveen, Ankit, R. Mayank, K. R. Mohit, A. J. Rohit and M. Nripan, *Nanoscale*, 2017, **9**, 14990–14997.

7 K. Takayoshi, O. Takaki, H. Misako, M. Taku and O. Hiromichi, *Sci. Rep.*, 2016, **6**, 25819.

8 M. G. Helander, Z. B. Wang, J. Qiu, M. T. Greiner, D. P. Puzzo, Z. W. Liu and Z. H. Lu, *Science*, 2011, **332**, 6032.

9 D. W. Mohammeda, R. B. Ameena, K. A. Sierrosb, J. Bowenc and S. N. Kukurekaa, *Thin Solid Films*, 2018, **645**, 241–252.

10 K. Eun-Hye, K. Hyo-Joong, L. Sang-Jin, L. Jae-Heung and K. Han-Ki, *RSC Adv.*, 2016, **6**, 46634–46642.

11 P. Jeong-Il, H. J. Hyuck, P. Sung-Hyun, H. K. Il, J. H. Gee, I. H. Sang and K. Han-Ki, *J. Power Sources*, 2017, **341**, 340–347.

12 P. Sung-Hyun, L. Sang-Mok, K. Eun-Hye, K. Tae-Ho, N. Yoon-Chae, L. Sang-Jin, L. Jae Heung and K. Han-Ki, *Sci. Rep.*, 2016, **6**, 33868.

13 K. Akshay and Z. Chongwu, *ACS Nano*, 2010, **4**, 11–14.

14 E. Klaus, *Nat. Photonics*, 2012, **6**, 809–817.

15 G. Xiaoyang, L. Xingyuan, L. Fengyuan, L. Hailing, F. Yi and Z. Nan, *Sci. Rep.*, 2015, **5**, 10569.

16 H. Xiao, Z. Zhiyuan, B. Shuyu, W. Mengfei, Q. Xiaoying, F. Zhanxi and Z. Hua, *Nat. Commun.*, 2013, **4**, 1444.

17 H. Sukjoon, Y. Junyeob, K. Gunho, K. Dongkyu, L. Habeom, K. Jinhyeong, L. Hyungman, L. Phillip and K. H. Seung, *ACS Nano*, 2013, **6**, 5024–5031.

18 H. Bing, P. Ke, H. Yuanlin, Z. Xiaojian, R. Qikun, L. Qinggeng, G. Yangfei, S. Tianyi, G. Chuanfei, C. David, G. Michael, W. Yang, G. Jinwei, R. Zhifeng and K. Krzysztof, *Adv. Mater.*, 2014, **26**, 873–877.

19 M.-M. Monica, D. W. Stefaan, W.-R. Rachel, W. A. Joel and B. Christophe, *Adv. Mater.*, 2017, **3**, 1600529.

20 A. Parretta, M. L. Jayaraj, A. D. Nocera, S. Loreti, L. Quercia and A. Agati, *Phys. Status Solidi A*, 1996, **155**, 399–404.

21 J. Deuermeier, J. Gassmann, J. Brotz and A. Klein, *J. Appl. Phys.*, 2011, **109**, 113704.

22 C. Zhu, A. Osherov and M. J. Panzer, *Electrochim. Acta*, 2013, **111**, 771–778.

23 K. Dong-Ju, K. Hyo-joong, S. Ki-won, K. Ki-hyun, K. Tae-Wongm and K. Han-Ki, *Sci. Rep.*, 2015, **5**, 16838.

24 D. Tahir and S. Tougaard, *J. Phys.: Condens. Matter*, 2012, **24**, 175002–175010.

25 J. Jin-A, K. Jihoon and K. Han-Ki, *Sol. Energy Mater. Sol. Cells*, 2011, **95**, 1974–1978.
26 J. Jin-A, K. Han-Ki and K. Jihoon, *Sol. Energy Mater. Sol. Cells*, 2014, **125**, 113–119.
27 D. S. Ghosh, T. L. Chen and V. Pruneri, *Appl. Phys. Lett.*, 2010, **96**, 041109.
28 G. Haacke, *J. Appl. Phys.*, 1976, **47**, 4086–4089.
29 C. Kyung-Su and K. Han-Ki, *RSC Adv.*, 2018, **8**, 2599–2609.
30 K. Yuna, K. Yoonjung, K. Sehwan and K. Eunkyoung, *ACS Nano*, 2010, **4**, 5277–5284.
31 K. Tae-Ho, S. Seok Hyun, K. Hyo-Jae, O. Seong-Hyeon, H. Song-Yi, K. Goung and N. Yoon-Chae, *Appl. Surf. Sci.*, 2018, **442**, 78–82.
32 J. Jacob, H. Markus, K. Inyoung, Y. Jong-Su, J. Jeongdai and K. Frederik C., *Adv. Funct. Mater.*, 2014, **24**, 1228–1233.
33 P. Qibing, Z. Guido, A. Markus and I. Olle, *Polymer*, 1994, **35**, 1347–1351.
34 C. Guofa, D. Peter, C. Mengqi, W. Jiangxin, C. Jingwei, M. Shlomo and L. Pooi See, *Adv. Energy Mater.*, 2016, **6**, 1501882.